Crescent singularities in crumpled sheets

Tao Liang and Thomas A. Witten

The James Franck Institute and the Department of Physics, The University of Chicago, 5640 S. Ellis Avenue,
Chicago, Illinois 60637, USA
(Received 18 July 2004; published 20 January 2005)

We examine the crescent singularity of a developable cone in a setting similar to that studied by Cerda *et al.*, [Nature (London) **401**, 46 (1999)]. Stretching is localized in a core region near the pushing tip and bending dominates the outer region. Two types of stresses in the outer region are identified and shown to scale differently with the distance to the tip. Energies of the d cone are estimated and the conditions for the scaling of core region size R_c are discussed. Tests of the pushing force equation and direct geometrical measurements provide numerical evidence that core size scales as $R_c \sim h^{1/3} R^{2/3}$, where h is the thickness of sheet and R is the supporting container radius, in agreement with the proposition of Cerda *et al.* We give arguments that this observed scaling law should not represent the asymptotic behavior. Other properties are also studied and tested numerically, consistent with our analysis.

I. INTRODUCTION

As we crumple a piece of paper in our hands, two types of singular structures appear in the crumpled paper: folding ridges and pointlike vertices. Energies are condensed into a network of such singularities. The properties of ridges have been studied thoroughly. Scaling laws governing the energy and size of the ridge have been obtained analytically and tested numerically [1–4]. Pointlike singularities are also studied extensively [5–12]; however, current understanding of their properties is not as complete as that of ridges.

In this paper, we consider a single conical vertex studied by Cerda *et al.* [5,6]. One experimental realization is to push the center of a circular elastic sheet of radius R_p axially into a cylindrical container of radius R, as illustrated in Fig. 1. This is the simplest volume-restricting deformation of the sheet and causes the center of the sheet to move into the container by a distance d. It is useful to express the deflection of the sheet by $\epsilon \equiv d/R$. Due to the constraint of unstretchability, the sheet deforms into a nonaxisymmetric conical surface which is only in partial contact with the edge of the container. In the limit that the thickness h of the sheet goes to zero, since the bending modulus $(\sim h^3)$ vanishes faster than the stretching modulus $(\sim h)$, there would be pure bending over the sheet and Gaussian curvature would be zero everywhere. Mathematically, such a conical surface is called a perfectly developable cone [13] (d cone). In this limit, some models about the shape of the d-cone have been proposed [6–8,12]. These models only give outer-region solutions of d-cone shape, in the sense that they do not consider the stretching energy that is inevitable on a real sheet with finite thickness. For a real sheet, it must stretch near the tip, because otherwise, the curvature at the tip would be divergent, since curvature goes as $1/r$, where r is the distance to the tip, thus causing divergent energy. Therefore, it is the finite thickness that causes the sheet to stretch greatly in a small region near the tip. This small region is called the core region. It is where energetically expensive stretching is localized and its size is governed by the competition of the bending and stretching energies of the whole cone. As a result of the stress focusing in the core region, crescentlike shapes come out where bending stresses are big, as shown in Fig. 2. In addition, as we will see later, finite thickness also causes a small amount of strains in the outer region.

One problem of great interest is concerned with the size of the core region, characterized by the radius of curvature of the crescents. We want to know whether there is scaling behavior of the core size and to determine any scaling exponents. Intuitively, we expect that this size R_c should have a dependence on thickness h, since R_c goes to zero as h goes to zero. Cerda *et al.* [5] propose that R_c scales as $R_c \sim h^{1/3} R^{2/3}$. This says that, besides h, the supporting container radius R also determines R_c. This is surprising because stretching energies are supposed to be localized in the core region, so the core should not be able to know about the length of outside container radius. In this work we explore this problem as well as other properties of a d cone. In Sec. II, we describe
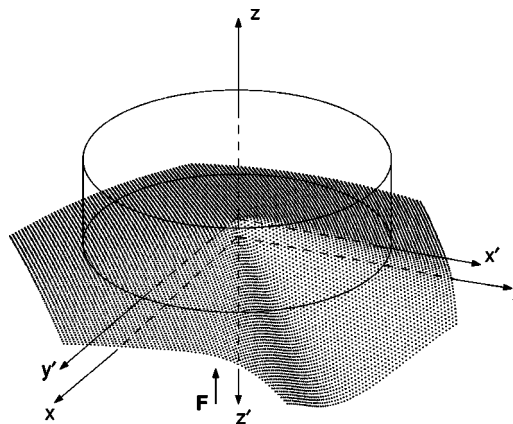

FIG. 1. A d cone appears when we push the center of an originally flat sheet against the edge of a cylindrical container from below with force F. This is a typical simulated d-cone shape, with side length $l=60a$, container radius $R=38a$, displacement $d=0.15R$, and thickness $h=0.102a$, where a is the lattice spacing. Two sets of coordinate systems are shown.
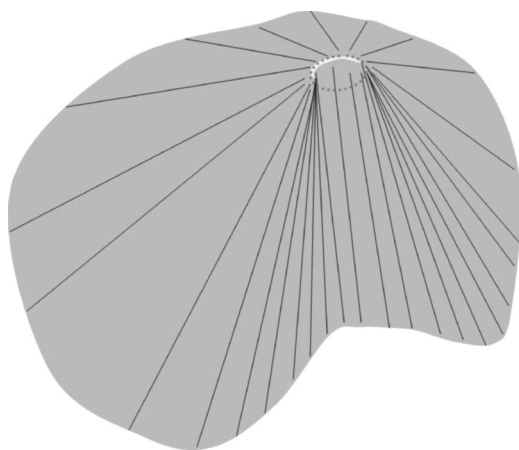
FIG. 2. Sketch of the core region of a d cone. The crescent area is shown in white. Directors are shown as black lines. Many directors converge toward the two tips of the crescent. The dashed circle tangent to the crescent at its center defines the radius R_c.

the energies and forces that give rise to the crescent singularity. We first study the elastic properties of a truncated d cone formed by cutting a cap region at the center of a regular d cone and then investigate the energetic variations as we join the cap region into the truncated d cone. From them, we discuss the conditions for the existence of scaling behavior of R_c. Details of numerical models of simulating an elastic sheet and producing desired shapes are presented in Sec. III. After numerical results that agree with the predicted d-cone properties are shown, we use two different methods to look for scaling exponents of R_c. Finally, the limitations of and implications from our findings and future work are discussed in Sec. IV.

II. THEORIES

We begin by stating the connection between the deformation of the sheet and its elastic energy. In a thin d cone the dominant energy is due to the bending distortion in outer region far from the crescent. We discuss the form of this energy and the stresses associated with it. Next we outline the energetic effects of the crescent region. Finally, we focus on how each of these energies is influenced by a change in the crescent radius R_c. We sketch how scaling properties of the energy produce scaling behavior in the sheet.

We first specify two coordinate systems. We define x-y as the horizontal plane of the supporting cylindrical container's edge, with the origin on the axis of cylinder and z axis pointing upward (see Fig. 1). We then define an x'-y' plane as parallel to the x-y plane but with origin at the tip of the sheet and z' axis pointing opposite to z axis. The x'-y' plane is displaced from the x-y plane by a distance d. Next we define (ρ, θ) as the polar coordinates in the x'-y' plane. In the cylindrical coordinates $\{\rho\theta z'\}$, the d cone is described by $z' = \rho\psi(\theta)$, in the limit that thickness $h \rightarrow 0$. We shall denote this limiting surface as the *asymptotic d cone*.

In equilibrium, the sheet assumes a conformation that minimizes the elastic energy. Thus, the actual core radius is

that which minimizes this energy. Two forms of energy must be considered: bending energy B and stretching energy S. The bending energy density is proportional to the square of the total curvature $C(r)$ [14]. This $C(r)$, defined as the trace of the curvature tensor, is sometimes called the mean curvature [15]. The constant of proportionality is called the bending modulus κ. Thus,

$$B = \frac{1}{2}\kappa \int dA C(r)^2, \tag{1}$$

where $\int dA$ denotes the integral over the surface. In general there is a second form of bending energy, proportional to the average Gaussian curvature. We show later in this section that this Gaussian curvature energy is unimportant for the present system.

The stretching energy density is proportional to the square of the strain tensor γ. For an isotropic material, there are two forms of stretching energy with constants of proportionality Yh and $Y_1 h$ [16]:

$$S = \frac{1}{2} \int dA[Yh(Tr\gamma)^2 + Y_1 h(Det\ \gamma)], \tag{2}$$

where Y is Young's modulus and Y_1 is a convenient combination of Y and dimensionless Poisson's ratio ν. They are related to bending modulus through $\kappa = Yh^3/12(1-\nu^2)$.

The actual strain and curvature fields are those which minimize the $B+S$. The variational minimization amounts to a statement that the normal forces on each element must balance. This statement is known as the "force von Kármán equation"

$$\partial_\alpha \partial_\beta M_{\alpha\beta} = \sigma_{\alpha\beta} C_{\alpha\beta} + P, \tag{3}$$

where $M_{\alpha\beta}$ are torques per unit length, $\sigma_{\alpha\beta}$ are in-plane stresses, and P is external force per unit area of the sheet.

When we push a circular sheet of radius R_p into a container to form a d cone, strain and curvature distortions are created and elastic energy is stored. This energy arises from several effects. It is convenient to discuss it by creating the final surface in two stages. In the first stage, we assume a value for R_c and cut a circular hole of that radius in the center of the sheet. We then force this perforated sheet into the container by exerting tension on the inner edge of the hole. In the unstretchable limit $h \ll R$, this shape becomes a truncated d cone, which serves as the outer region of a regular d cone. In this region, the curvature at every point vanishes in the radial direction. The total curvature C has the form $C = \phi(\theta)/r$. Its bending energy B_0 is thus given by

$$B_0 = \frac{1}{2}\kappa \int_{R_c}^{R_p} rdr/r^2 \int d\theta\phi^2(\theta) \propto \kappa \ln(R/R_c). \tag{4}$$

In the limit $h \ll R_c \ll R_p$, this B_0 dominates the energy, as we justify below. Then the function ϕ takes the form that minimizes B_0 subject to the constraints on the d cone. In this geometry, the force von Kármán equation simplifies greatly, and the form of $\phi(\theta)$ as well as the associated stresses can be found explicitly [6,12].

We first determine the transverse stress $\sigma_{\theta\theta}$ using Eq. (3). The nonzero components of torque tensor M follow from the constitutive law implicit in the energy equations [14]: $M_{rr} = \kappa\nu C_{\theta\theta} = \kappa\nu\phi(\theta)/r$ and $M_{\theta\theta} = \kappa C_{\theta\theta} = \kappa\phi(\theta)/r$. The force von Kármán equation then reduces to $\partial_r^2 M_{rr} + \partial_\theta^2 M_{\theta\theta}/r^2 = \sigma_{\theta\theta}C_{\theta\theta} + P$, from which we obtain

$$\sigma_{\theta\theta} = \frac{\kappa}{r^2}\left(2\nu + \frac{\ddot{\phi}(\theta)}{\phi(\theta)}\right) - \frac{Pr}{\phi(\theta)}, \qquad (5)$$

where the overdots denote θ derivatives. In the same region where only $C_{\theta\theta}$ is nonzero, there is no pressure from external force acting on the sheet—i.e., $P=0$. Therefore, according to Eq. (5), the stress $\sigma_{\theta\theta}$ goes as κ/r^2. These stresses arise from the requirement that the normal force due to changing torques be balanced by the normal force due to in-plane tension of the sheet. We call them type-I stresses and denote them by the symbol $\sigma^{(1)}$.

On the other hand, we consider the force balance of a region that encloses the area between the inner radius R_c and outer radius r, where r can take values between R_c and R. The tension exerted on the inner edge of this region is equivalent to the central pushing force of a regular d cone. This force must be balanced by the force due to radial in-plane stress σ_{rr} on the outer perimeter of the region. Let β be the angle between a radial line or generator of the d cone and the horizontal. Since $\tan\beta = \psi(\theta)$, we have $\sin\beta = \psi(\theta)/\sqrt{1+\psi^2(\theta)}$. The balance of vertical forces yields

$$\int \sigma_{rr} r \sin\beta d\theta = F, \qquad (6)$$

which holds for every value of r from R_c to R. It is easy to see that type-I stresses alone cannot satisfy this equation; since type-I stresses go as $1/r^2$, they would give a $1/r$ prefactor on the left side of equation, while the right side of the equation is independent of r. Therefore, the integral from type-I stresses must vanish and there must exist some additional stresses in the outer region that scale as $1/r$ to satisfy Eq. (6). We call these stresses type-II stresses and denote them by $\sigma^{(2)}$. They persist up to the supporting container edge, where normal force from the container counteracts the external pushing force. We can write $\sigma^{(2)}r = Fe(\theta)$, where $e(\theta)$ is a function only of θ and satisfies $\int e(\theta)\sin\beta d\theta = 1$. It is obvious that $e(\theta)$ is of order unity.

To estimate the magnitude of type-II stresses, we notice that $F = \partial E/\partial d = (\partial E/\partial \epsilon)/R \approx \kappa/R$. Thus $\sigma^{(2)} \approx F/r \approx \kappa/(rR)$. The type-II stresses are comparable with type-I stresses only near the container edge since the ratio $\sigma^{(1)}/\sigma^{(2)} \approx r/R$ for $R_c < r < R$. It is noted that they are both due to nonzero thicknesses. Since in-plane stress tensors are related to strain tensors through [16] $\sigma_{\alpha\beta} = [Yh/(1-\nu^2)](\gamma_{\alpha\beta} + \nu\epsilon_{\alpha\rho}\epsilon_{\beta\tau}\gamma_{\rho\tau})$, we have strains $\gamma \approx \sigma/(Yh)$. The stretching energy of a truncated d cone is then

$$S_0 \approx \kappa h^{-2} \int [(\sigma^{(1)} + \sigma^{(2)})/(Yh)]^2 r dr d\theta \approx \kappa h^2/R_c^2. \quad (7)$$

We now examine the profile of the external force along the container edge. Here the external normal force pressure P of Eq. (3) is nonvanishing. This normal force causes a small transverse deflection of the sheet and hence induces both curvature and strain near the edge. Noticing that the curvature induced is in the radial direction and has opposite sign with $C_{\theta\theta}$, we expect the mean curvature to be reduced near the edge. Due to the translational symmetry along the region of the surface in contact with the cylindrical container, the normal force pressure is found to be independent of the azimuthal angle θ. However, besides this θ-independent term, Cerda and Mahadevan [12] show that a δ-function term of θ emerges in the normal force pressure expression in order to make the torque balance, and this singularity happens at the take-off angular positions, where the sheet begins to bend away from the container. Since stresses and curvatures should avoid singular behavior for the sake of energy, according to Eq. (5), there must exist a δ-function term in $\ddot{\phi}(\theta)$ to cancel that from normal force pressure P. Integrating over θ, we conclude that $\dot{\phi}(\theta)$ should have a jump at the take-off positions. This result is consistent with the geometrical requirement. More quantitatively, following Ref. [12], we find that the ratio of the normal force contributed by the δ-function term to that contributed by the θ-independent term is $\tan\theta_c/[2(\pi-\theta_c)]$, where θ_c is the half aperture angle of the noncontact region. For small deflections, taking $\theta_c \approx 1.21$ rad [6], we obtain the value of this ratio, 0.69. We will numerically verify this ratio later.

Having discussed stresses and forces, we now consider in detail the bending energy B_0. The bending energy comes from both the total curvature and Gaussian curvature. Since the truncated d cone has no Gaussian curvature, we only need to take account of the total curvature contribution. The reduced curvature $\phi(\theta)$ is related to the reduced height $\psi(\theta) \equiv z'/\rho$ defined in the beginning of this section: $\phi(\theta) = \psi(\theta) + \ddot{\psi}(\theta) - \psi(\theta)\dot{\psi}^2(\theta)/[1+\psi^2(\theta)]$. For small to moderate deformations of the sheet ($\epsilon \lesssim 0.4$), $C \approx (\psi+\ddot{\psi})/r \approx \epsilon/r$. Throughout the paper we shall focus on this moderate range of ϵ. The bending energy B_0 has the form

$$B_0 = \frac{\kappa}{2}\int C^2 dA \approx G_1 \kappa \epsilon^2 \ln(R_p/R_c), \qquad (8)$$

where G_1 is a geometrical factor. Comparing this with S_0 from Eq. (7), we see that bending dominates the outer region.

Although Gaussian curvature is zero everywhere in a truncated d cone, it is certainly not the case for a regular d cone. The Gaussian curvature contribution to the bending energy is $B_G = (\kappa_G/2)\int K dA$, where κ_G is the Gaussian curvature coefficient, K is the Gaussian curvature, and A is the area. According to the Gauss-Bonnet theorem, the integral of Gaussian curvature over a region M of a surface is related [13] to the integral of the geodesic curvature κ_g over the boundary of that region through $\int_M K dA = 2\pi - \int_{\partial M}\kappa_g ds$. Choosing M to be the whole sheet without perforation, we get $B_G = (\kappa_G/2)(2\pi - \int\kappa_g ds)$. If the sheet were a perfectly developable conical surface, the geodesic curvature at the perimeter would be the same as that of a regular cone of the
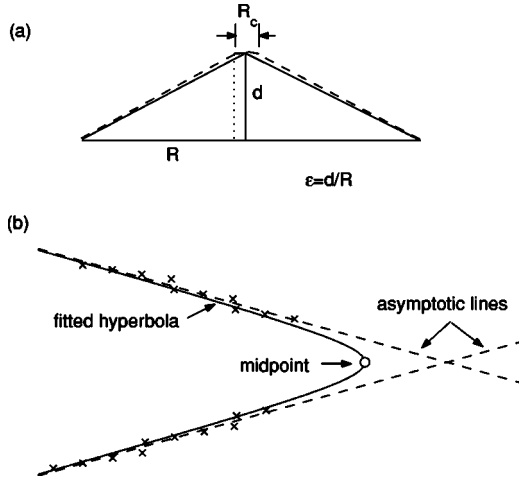
FIG. 3. (a) Sketch of a cross section of the d cone. The solid hypotenuse is for the d cone when $h \to 0$ and has slope ϵ; the dashed hypotenuse is for a real sheet ($h \neq 0$) and has slope ϵ'. (b) Sketch of fitting a hyperbola to find R_c from geometry.

same size: $\kappa_g = 1/R_p$, where R_p is the perimeter-to-tip distance. However, due to stretching of the real sheet and pushing of the container edge, the shape is not perfectly developable, so there are variations in the perimeter-to-tip distances along the boundary which make κ_g deviate from $1/R_p$. Since stretching is small compared with bending and the sheet is nearly developable over most of the surface, this deviation is small compared with $1/R_p$, and it should depend on the thickness h. We suppose that κ_g is a regular function of h and may be expressed as $\kappa_g \approx (1/R_p)[1 + (h/R_p)\Theta(\theta, \epsilon)]$, where Θ is a dimensionless function of θ and ϵ. Substituting this into the equation for the bending energy, we obtain $B_G = -(\kappa_G/2)(h/R_p)\int \Theta(\theta, \epsilon)d\theta$. Compared with Eq. (8), this energy is only a small fraction $(h/R_p)/\ln(R_p/R_c)$ of the bending energy contributed by the total curvature.

The truncated d cone discussed above has no crescent singularity. This singularity arises from the further constraints of filling in the hole in the truncated cone. The flat disk of radius R_c that was removed must be distorted in order to join onto the truncated cone. This distorted cap exerts forces on the truncated d cone and distorts it in turn. All of these distortions add elastic energy to the energy $B_0 + S_0$ of the initial truncated d cone. One obvious addition is the bending energy B_G due to Gaussian curvature discussed above. Another simple consequence of adding the core region is to alter the slope of the outer region generator from ϵ to a higher value ϵ' as shown in Fig. 3(a). To relate ϵ' to ϵ, we imagine a cross section of the d cone extending from the container edge to the tip and back down to the edge [see Fig. 3(a)]. In the truncated d cone, the generators have the same slope ϵ as the straight line from the container edge to the vertex, as shown by the solid lines in Fig. 3(a). Now, for the real sheet, the cap is curved, with a curvature radius of order R_c, but still, its uppermost point remains at height d. This rounding at the top necessarily increases the slope of the outer cone generator, as illustrated by the dashed lines in the same figure. When deformation is small, $\epsilon' \approx d/(R - R_c/2) \approx \epsilon[1 + R_c/(2R)]$. The altered bending energy is given by Eq.

(8) with ϵ replaced by ϵ': $B_0' \approx G_1 \kappa \epsilon^2 (1 + R_c/R)\ln(R_p/R_c)$. This increases the B_0 energy by a factor $(1 + R_c/R)$. This addition to the energy favors small R_c.

Besides these variations, there are other forms of added energy. We denote them as ΔE. It consists of stretching energy ΔE_0 added to the original region plus the energy E_c of the cap or core region. The added energy ΔE is expected to be much smaller than the dominant energy B_0 discussed above. Nevertheless, ΔE is all important in determining the core radius R_c.

Further distortions increase the energy of the outer region. The crescent singularity increases the curvature near the tips of the crescent. As shown in Fig. 2, the generators, initially distributed smoothly around the inner hole, are now concentrated at the tips of the crescent, increasing the curvature there. The generators splay outward from these tips. Observation suggests that a finite fraction of the generators are pushed to the tips. These generators appear to splay outward less rapidly when the size R is increased. These observations suggest that (a) the crescent increases the exterior curvature energy and (b) this energy decreases as the size $R \to \infty$ for a given R_c. This energy penalty favors small R_c/R. We do not have a more specific estimate for this energy at present.

We now consider the energy E_c of the cap or core region itself. In order to bridge the truncated cone, the average curvature C must be of order ϵ/R_c. If the curvatures are uniform, the associated bending energy is of order $\kappa \int dA C^2 \simeq \kappa \epsilon^2$. However, such uniform curvatures are not optimal. The smoothly curved cap region has typical Gaussian curvatures of order ϵ^2/R_c^2, consisting of a negative part in the buckled region and a comparable positive part elsewhere. The presence of Gaussian curvature induces strain of order ϵ^2 and a stretching energy of order $\kappa h^{-2}\epsilon^4 R_c^2$. The system may alleviate this large stress energy by concentrating the curvature, as in the simple stretching ridge [3]. The observed crescent singularity is presumably the result of this concentrated curvature. The length of this crescent is of order R_c; its width w is evidently that which minimizes E_c. If w is a fixed fraction of R_c, the above estimates show that E_c grows as R_c^2. To improve this energy, w/R_c must go to zero as R_c grows. The total curvature is then of order $1/w$, and the bending energy of the core goes as $\kappa w R_c/w^2 \sim R_c/w$. This energy must grow indefinitely as $R_c \to \infty$. Evidently, the core energy favors small R_c.

With these energies in mind, we now investigate how R_c is determined. It is clear that R_c is controlled by the competition of energies. The total energy is $E = S_0 + B_0' + B_G + \Delta E$. Our purpose is to find an optimal R_c that minimizes the total energy. First, taking the derivative of B_0' with respect to R_c, we have $\partial B_0'/\partial R_c = G_1 \kappa \epsilon^2 \{-1/R_c + [\ln(R_p/R_c) - 1]/R\}$. In the regime of interest, R is comparable with R_p, and $R_c \ll R$, so the first term dominates the second term: $\partial B_0'/\partial R_c \approx -G_1 \kappa \epsilon^2/R_c$. This implies that B_0 favors large R_c. Next, we notice that since $\partial B_G/\partial R_c$ and $\partial S_0/\partial R_c$ are much smaller than $\partial B_0'/\partial R_c$ in this regime, the competition happens mainly between the outer bending energy B_0' and the added energy ΔE. Though we know little about the form of the added energy ΔE, the above observations suggest that (a) it favors small R_c, (b) it decreases as R increases, and (c) it involves stretch-

ing, and thus increases with decreasing thickness h. To illustrate the possible effect of this energy, we posit that ΔE is homogeneous in R_c, R, and h:

$$\Delta E = \kappa g(\epsilon) R_c^s R^{-t} h^{-s+t}, \quad (9)$$

where $g(\epsilon)$ is an unknown function of ϵ and s and t are unknown positive exponents. The h power law is determined from s and t by dimensional consistency. The energy minimization with respect to the variational parameter R_c then implies

$$0 = R_c \frac{\partial E}{\partial R_c} = - G_1 \kappa \epsilon^2 + s \Delta E. \quad (10)$$

Using the assumed power-law form of ΔE, we infer

$$R_c \sim R^{t/s} h^{1-t/s}. \quad (11)$$

Thus the assumption of Eq. (9) implies that R_c should increase as a power of R. Since R_c cannot exceed R, the power must be smaller than unity, so that t must be smaller than s.

Though this assumed form for ΔE gives a pleasing result, we warn that it cannot be correct in the limit of large R/h. If it were correct, it would imply that R_c/h goes to infinity with R/h. This implies that the core energy E_c must go to infinity relative to $\kappa \epsilon^2$, as shown above. The increase of E_c occurs irrespective of R. Thus E_c must grow to dominate the total energy. Such a large E_c is not compatible with a minimum of total energy. It must be balanced by some other energy favoring large R_c. No such energy is apparent. Thus R_c cannot grow indefinitely. Conversely, any observed power-law growth of R_c must cease for sufficiently large R/h. In the numerical section, we will give an empirical discussion of the range of R/h in which the scaling of R_c holds.

These conclusions contrast with the scaling argument proposed in the initial studies of the d cone [5,12]. Thus it is important to revisit this scaling argument and show how the contradiction with our result arises. The authors attribute the scaling to an energy balance between bending and stretching in the core region. To estimate the stretching energy, they consider a director traversing the sheet from one edge, through the core and on to the opposite edge, such as the dashed line in Fig. 3(a). They note that increased R_c increases the length of this chord (relative to the solid line) by a fraction of order $(R_c/R)^2$. If this strain is presumed uniform, the associated stretching energy in the core is of order $\kappa h^{-2} R_c^2 (R_c/R)^4$. They balance this energy against the bending energy in the core, presumed to be of order $\kappa \epsilon^2$. This balance yields $R_c \sim R^{2/3} h^{1/3}$.

This argument seems questionable, since it ignores energies much larger than the ones it includes. Its assumption of uniform strain leads to a stretching energy of uniform density outside as well as within the core. The argument includes that part of this energy lying within the core while ignoring the much larger part outside the core. If one tries to repair the estimate by supposing the excess length resides only in the core, then the strain becomes independent of R and the R_c must be independent of R. In addition the argument ignores the large stretching energy in the core arising from the necessary Gaussian curvature within the core itself, as discussed

above. Likewise, it takes no account of the strong difference between the two principal curvatures in the crescent.

Our analysis of the energy given above allows us to infer the scaling of R_c based on measurements of the central pushing force F. The inference is valid as long as the dominant energy is the B_0 energy above. The energy balance equation (10) allows us to write $\Delta E = G_2 \kappa \epsilon^2$, where G_2 is a numerical constant. Thus,

$$E \approx G_1 \kappa \epsilon^2 \ln(R_p/R_c) + G_2 \kappa \epsilon^2. \quad (12)$$

The pushing force follows from $F = \partial E / \partial d = (\partial E / \partial \epsilon)/R$. To explore the scaling of R_c, we write R_c as $R_c = h^p R^q R_p^\lambda A(\epsilon)$, where p, q, and λ are scaling exponents to be determined and $A(\epsilon)$ is a function only of ϵ. Dimensional consistency requires that $p+q+\lambda=1$. Previous work [5,6] did not consider the possibility that R_c has a dependence on R_p. Here we address it by introducing λ. From Eq. (12) and the scaling expression of R_c, the pushing force is calculated to be

$$F \approx \frac{2 G_1 \kappa \epsilon}{R} [- p \ln h - q \ln R + (1 - \lambda) \ln R_p + f(\epsilon)], \quad (13)$$

where $f(\epsilon) = -\ln A(\epsilon) + G_2/G_1 - \epsilon \dot{A}(\epsilon)/2A(\epsilon)$ is a function only of ϵ. We will use this equation to test the scaling relations in the numerical section, which follows below.

III. NUMERICS AND FINDINGS

A. Numerical model

We model an elastic sheet by a triangular lattice of springs of unstretched length a and spring constant k after Seung and Nelson [15]. Bending rigidity is introduced by assigning an energy of $J(1 - \hat{n}_1 \cdot \hat{n}_2)$ to every pair of adjacent triangles with normals $\hat{n}_1$ and $\hat{n}_2$. When strains are small compared to unity and radii of curvature are large compared to the lattice spacing a, this model is equivalent to an elastic sheet of thickness $h = a\sqrt{8J/k}$ made of an isotropic, homogeneous material with bending modulus $\kappa = J\sqrt{3}/2$, Young's modulus $Y = 2ka/h\sqrt{3}$, and Poisson's ratio $\nu = 1/3$. The lattice spacing a is set to 1. The shape of the sheet in our simulation is a regular hexagon of side length R_p. The typical value of R_p is $60a$.

To obtain a single d-cone shape, we need to simulate the constraining container edge and pushing force. As shown in Fig. 1, the edge lies in the x-y plane and is described by the equation $x^2 + y^2 = R^2$. Pushing in the center of the sheet is accomplished by introducing a repulsive potential of the form $U_{\text{force}}(z_1) = -F z_1$, where z_1 is the z coordinate of the lattice point in the center and F is the magnitude of the pushing force. This force is applied in the positive z direction. The constraining edge is implemented by a potential of the form $U_{\text{edge}} = \Sigma C_p H(z_i)/\{[(\sqrt{x_i^2 + y_i^2} - R)^2 + z_i^2]^4 + \xi^8\}$, where ξ, C_p are constants and the summation is over all lattice points with coordinates (x_i, y_i, z_i). $H(z)$ is the unit step function, which makes certain that this potential only acts on the lattice points that have already moved into the container (those with $z_i > 0$). The force associated with it decays rapidly once the lattice points go away from the edge. The con-

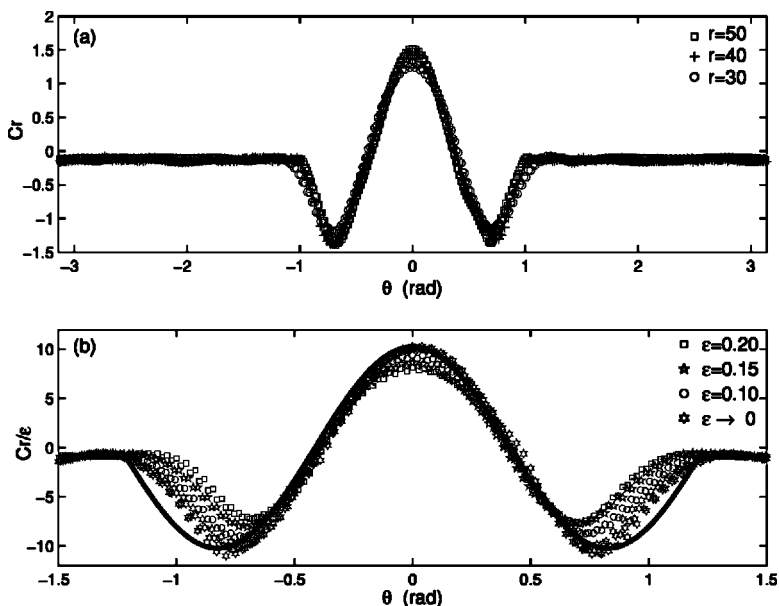FIG. 4. (a) Azimuthal profile of normalized total curvature on a d cone at three fixed distances from the tip. Curvature is positive for the concave region, negative for the convex region. Curvature is normalized by $1/r$, where r is the fixed distance from the tip. This plot is for the d-cone shape shown in Fig. 1 at distances $30a$ (circle), $40a$ (plus), and $50a$ (square) from the tip. The container touches the d-cone surface at $r = R\sqrt{1+\epsilon^2} \approx 38.4a$. (b) Normalized curvature profiles for four different values of ϵ at fixed thickness $h=0.102a$. Curvature is normalized by ϵ/r. The profile at $\epsilon \to 0$ is obtained by extrapolating from profiles at $\epsilon=0.10$, 0.15, and 0.20. The solid line is the exact solution as both $h \to 0$ and $\epsilon \to 0$ [6,12].

jugate gradient algorithm [17] is used to minimize the total elastic and potential energies of the system as a function of the coordinates of all lattice points. Figure 1 shows one such minimized configuration of the lattice grid. The simulated sheet is indeed only in partial contact with the container edge. In the rest of this section, we shall first compare our results to the d-cone predictions of previous work. The good agreement indicates that our numerical realization is reliable. Next we shall investigate the scaling behavior of R_c.

B. Curvature profile

We first test our simulation by measuring the curvature profile of the sheet and comparing it to the prediction under certain limiting situations. We determine the curvatures approximately from each triangle in the sheet. For this measurement, we take the curvature tensor to be constant across each triangle. We calculate it using the relative heights of the six vertices of the three triangles that share sides with the given triangle [18]. The six relative heights w_i normal to the triangle surface are fit to a function of the form

$$w_i = b_1 + b_2 u_i + b_3 v_i + b_4 u_i^2 + b_5 u_i v_i + b_6 v_i^2, \quad i = 1, \ldots, 6,$$

$$(14)$$

where $\{u_i, v_i, w_i\}$ are coordinates of the vertices in a local coordinate system that has the w axis perpendicular to the surface of the given triangle. This choice of local coordinate system ensures that b_2 and b_3 are negligible so that curvature tensors can be determined only from the coefficients of quadratic terms. In practice, our numerical findings do show that the values of b_2 and b_3 are on the order of 10^{-2} or lower. Therefore, curvature tensors follow immediately from the identification $C_{uu} = 2 \times b_4$, $C_{vv} = 2 \times b_6$, and $C_{uv} = b_5$. The total curvature C is defined as the trace of the curvature tensor: $C = C_{uu} + C_{vv}$. Figure 4(a) gives a typical plot of the total curvature versus azimuthal angle on a d-cone surface at three different distances from the tip. Curvature is measured in units of $1/r$ and taken to be negative in the convex region,

where the sheet touches the supporting container. The three curves mostly collapse into one single curve. This roughly verifies that the curvature goes as $1/r$. However, near $\theta=0$, the normalized curvature becomes systematically smaller for smaller r. We attribute this departure to the influence of the stretched crescent region.

The shapes of the curves are in qualitative agreement with our analysis below. The surface is in contact with the container for angles θ larger than some θ_c in magnitude. For $|\theta| > \theta_c$, the normalized curvature at all r shown is constant and its value is that of a simple cone of the same ϵ. As $|\theta|$ becomes less than the "take-off" angle θ_c, the surface curves inwardly away from the container and the total curvature begins to increase in negative direction. The crescent singularity is most likely to live near the region where total curvature reaches its negative maximum. As $|\theta|$ decreases further, the curvature goes to zero, changes signs, and reaches a central positive maximum at $\theta=0$, which corresponds to where the sheet is maximally deflected.

As thickness h and deformation ϵ go to zero, Cerda and Mahadevan obtained the exact solution of curvature profile [6,12]. Although it is impossible for us to get the $h \to 0$ profile, we want to compare our data with their prediction in the limit that $\epsilon=0$. To do so, recall that the total curvature, as mentioned in Sec. I is related to the shape through $C = \{\psi(\theta) + \ddot{\psi}(\theta) - \psi(\theta)\dot{\psi}^2(\theta) / [1 + \dot{\psi}^2(\theta)]\}/r$. Since $\psi(\theta) \propto \epsilon$, we have $Cr/\epsilon = a_0 + a_1\epsilon^2 + a_2\epsilon^4 + O(\epsilon^6)$, where a_0, a_1, and a_2 could depend on θ. Hence, from this equation, we can extrapolate the curvature at $\epsilon=0$ by fitting the curvature at three known values of ϵ with basis functions $\{1, \epsilon^2, \epsilon^4\}$. In Fig. 4(b) we plot curvature profiles at $\epsilon=0.20$, 0.15, 0.10, and 0. The $\epsilon \to 0$ profile is extrapolated from other three profiles using the fitting theme discussed above. The solid line is the theory curve of exact solution. As we can see from this graph, as ϵ decreases, the curvature profile becomes closer to the theory curve, which is based on the assumption that $\epsilon=0$ and $h=0$. Our $\epsilon=0$ profile agrees well with the theory curve in the central peak region. However, a striking differ-
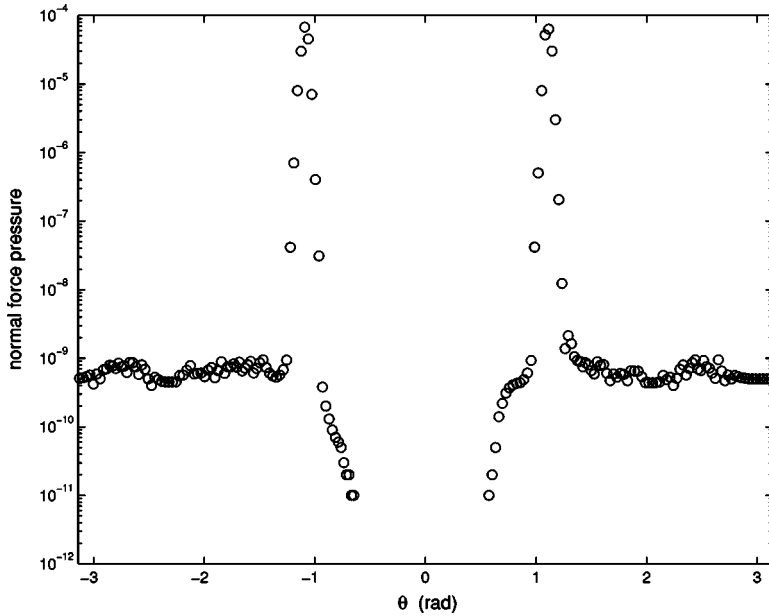
FIG. 5. Azimuthal profile of the normal force pressure. This is for the shape shown in Fig. 1. Normal force pressure is measured in relative units. The right peak is located at 1.12 rad; the left peak is located at −1.09 rad.

ence still exists in the range between the take-off positions and negative maxima. This discrepancy can be explained by the effect of nonzero thickness. For a real sheet, $h \neq 0$, from Eq. (5), we observe that $\dot{\phi}$ tends to avoid jump at take-off positions in the noncontact region where external pressure $P = 0$; otherwise, there would be a singularity in the strains. Therefore the observed curvature profile has to be rounded rather than having an abrupt kink in slope, which requires that the curvature profile be curved up as the sheet leaves the container, just like what is displayed in the plot. Besides, the same reason can explain the slight difference near take-off points in the curvature profiles at the three distances in Fig. 4(a). For smaller r, the curvature may be more influenced by a nonzero thickness effect, so the profile at $r = 30a$ is more rounded than the profile at $r = 50a$. In addition, we note that the theory curve based on the model proposed by Chaieb *et al.* [8] does not match our data.

From the curvature file, we can measure the opening angle of a d cone. The opening angle is defined as the angular distance between the two "take-off points" where the sheet loses contact with the container. For asymptotically thin sheets with small deformation, this angle is predicted to be 138° from the exact solution, as illustrated by the solid line of Fig. 4(b). As ϵ decreases to zero, the opening angle measured from curvature profiles tends to converge to that indicated by the solid line. We expect agreement with the prediction when the elastic thickness h vanishes. This value was approximately confirmed by experiments, which yielded 130° [6].

C. Normal force

The azimuthal profile of the normal force pressure from the container is displayed in Fig. 5. It is evident that we do observe sharp peaks at the take-off positions, which confirm the δ-function term in the normal force pressure proposed in [12]. The pressure drops quickly to zero as one enters the buckled region where the sheet bends away from container.

The angular separation of the take-off positions is about 2.21 rad = 127°. To verify that the sharp peaks in the normal force pressure have the proper strength, we calculate the ratio of the normal force from the δ-function term to that from the θ-independent term. The ratio is found to be 0.70 from our data, compared well with the theoretical prediction 0.69 obtained in Sec. II.

Our measurements in Sec. III B and this section confirm that our simulation accurately represents an elastic sheet as desired. We now report the observed behavior of the core region.

D. Scaling of the core size

To study the scaling law of the core region size, it is natural to start estimating the core size by finding the radius of curvature of crescents. From azimuthal profiles of curvature at different distances, we find the locations of the triangles with maximal negative curvature on both sides at each fixed distance. The centers of these triangles are projected onto the x-y plane. The best fitted straight lines to the projection points on two sides serve as the asymptotic lines of a hyperbola, and the central forcing point is taken as the midpoint of the same hyperbola. This process is illustrated in Fig. 3(b). R_c is the radius of curvature at the midpoint of the fitted hyperbola shape. Figure 6 shows the dependence of R_c measured in this way on h and R when deformation ϵ is fixed at 0.10 and 0.15. We can observe power-law dependence from these plots. The power-law fits give 0.334 ± 0.022 and 0.380 ± 0.014 for thickness dependence and give 0.574 ± 0.021 and 0.597 ± 0.032 for radius dependence. These values roughly agree with the 1/3 and 2/3 exponents proposed in Ref. [5].

As pointed out above, however, the lattice model can only accurately simulate an elastic sheet where the radius of curvature, $1/C$, is locally much greater than the lattice spacing. We expect this condition not to be well satisfied in the core region, where a singularity happens. Indeed, our data indi-
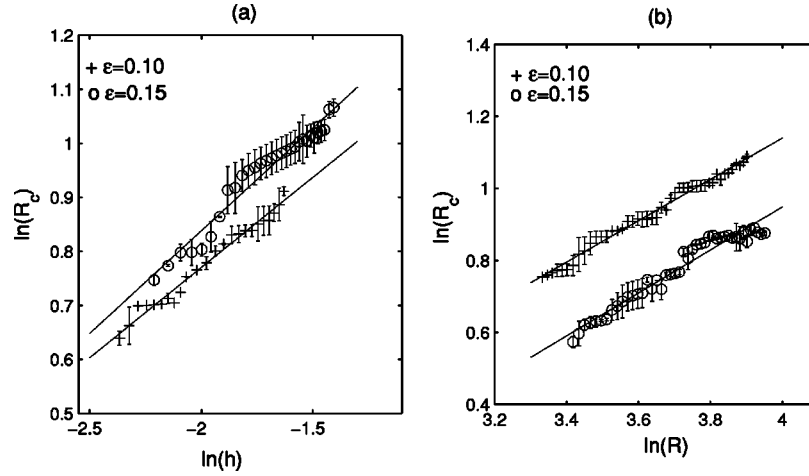
FIG. 6. The plots of (a) R_c versus h and (b) R_c versus R at $\epsilon=0.10$ and $\epsilon=0.15$. R is fixed for plots in (a); h is fixed for plots in (b). The straight lines are power-law fits. The fitted values of power in (a) are 0.334 ± 0.022 for $\epsilon=0.10$ and 0.380 ± 0.014 for $\epsilon=0.15$. The fitted values of power in (b) are 0.574 ± 0.021 for $\epsilon=0.10$ and 0.597 ± 0.032 for $\epsilon=0.15$. The error bars in the graph come from the numerical hysteresis effect when the thickness of the sheet or radius of the container is increased and decreased through the same value during the energy minimization process.

cate that Ca can be as big as 0.5 in this region even for small ϵ. Thus we have no hope of maintaining complete accuracy in this region. In addition, we find that the curvature data do not exhibit the kind of shape as shown in Fig. 4 at small distances. Therefore, in the above procedure of measuring R_c geometrically, we have to use curvature profiles at big distances, which makes it not so accurate to determine R_c in this way since R_c is supposed to be determined from the information in the neighborhood of the tip.

Our second approach of looking for the scaling relations is to use the force equation (13). In our simulation, we keep the spring constant k fixed ($k=1$), which is equivalent to fixing the two-dimensional Young's modulus (Yh) since we have $Yh=2ka/\sqrt{3}$. Hence $\kappa\propto Yh^3\propto h^2$. From Eq. (13) we have

$$F \approx \frac{h^2}{BR}[-p\ln h - q\ln R + (p+q)\ln R_p + D], \quad (15)$$

where B and D only depend on ϵ, which we now fix at 0.10. Fixing ϵ is realized through a process of several minimizations. We slowly adjust the pushing force until the desired ϵ value is reached. In every step of the process, the previously obtained minimized configuration is used as the input for the next minimization procedure.

To find the relations between exponents, we first fix h by fixing the bending coefficient J defined in Sec. III A and measure force F on the minimized shapes for different values of R. Figure 7(a) gives a semilogarithmic plot of FR versus R when h is fixed at $0.102a$ and R_p is fixed at $60a$. The linear feature of the plot agrees with the prediction from Eq. (15).
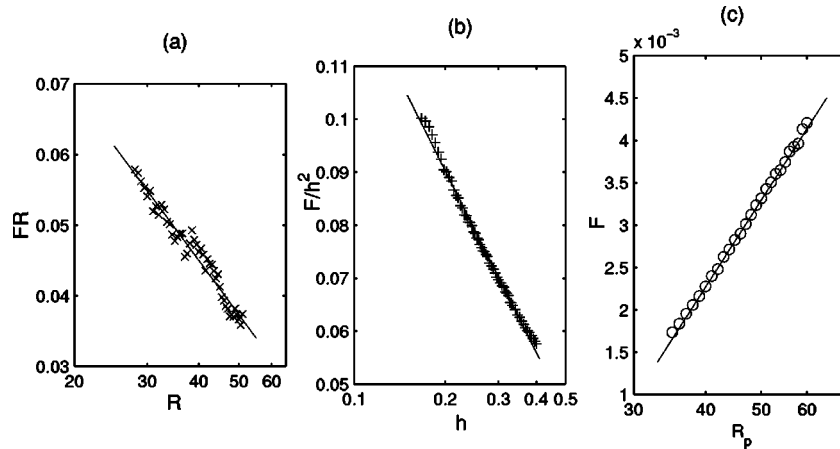

FIG. 7. Force plots when ϵ is fixed at 0.10. (a) FR versus R semilogarithmic plot. The data are fitted to be $FR=-0.0342\times\ln R +0.1714$. The parameters we use are $k=1$, $J=0.0013$, and $R_p=60a$. (b) F/h^2 versus h semilogarithmic plot. The data are fitted to be $F/h^2=-0.0494\times\ln h+0.0108$. The parameters we use are $k=1$, $R=37a$, and $R_p=60a$. (c) F versus R_p semilogarithmic plot. The data are fitted to be $F=0.0046\times\ln R_p-0.0147$. The parameters we use are $k=1$, $J=0.003$, and $R=25a$. The relation between exponents p and q is $q=1.879p$.

We denote the slope and intercept of the best-fitted line by S_1 and I_1, respectively. Then $S_1 = -0.0342 \pm 0.0011$ and $I_1 = 0.1714 \pm 0.0042$. From Eq. (15) we find

$$I_1 B = h^2[-p \ln h + (p+q)\ln R_p + D], \qquad (16a)$$

$$S_1 B = h^2(-q). \qquad (16b)$$

Next, for the same value of ϵ, $R = 37a$ and $R'_p = 60a$ are fixed while h is varied as the corresponding equilibrium force F is measured. The F/h^2 versus h semilogarithmic plot is shown in Fig. 7(b). Similarly the slope of the best-fitted line $S_2 = -0.0494 \pm 0.0005$ and intercept $I_2 = 0.0108 \pm 0.0006$, which according to Eq. (15) are given by

$$I_2 B = \frac{1}{R}[-q \ln R + (p+q)\ln R'_p + D], \qquad (17a)$$

$$S_2 B = \frac{1}{R}(-p). \qquad (17b)$$

Notice that Eqs. (16a), (16b), (17a), and (17b) constitute a homogeneous system of four linear equations in four variables $\{p, q, D, B\}$. In order to have nontrivial solutions, the determinant of its coefficient matrix must vanish. To check this condition, we write out the determinant of dimensionless matrix of coefficients explicitly:

$$\begin{vmatrix} (\ln R_p - \ln h) & \ln R_p & 1 & -I_1/h^2 \\ 0 & 1 & 0 & S_1/h^2 \\ \ln R'_p & (\ln R'_p - \ln R) & 1 & -I_2 R \\ 1 & 0 & 0 & S_2 R \end{vmatrix}$$

$$= (\ln R/h^2)S_1 + I_1/h^2 - [R \ln(hR'_p/R_p)]S_2 - RI_2,$$

which is calculated to be 0.016 ± 0.861, indeed including 0. In addition, we obtain the relations between these variables: $q = (1.879 \pm 0.428)p$ and $B = (0.547 \pm 0.005)p$.

The third relationship we can extract from force equation (15) is F versus R_p. To test this, we keep the $h_1 = 0.1549a$ and $R_1 = 25a$ fixed while measuring pushing forces for different R_p. The plot is shown in Fig. 7(c). On the one hand, the slope of the best-fitted line is 0.00461 ± 0.00003 and the intercept is -0.0147 ± 0.0001. On the other hand, we can calculate the slope and intercept of this graph using the relations between p, q, D, and B obtained above. Specifically, from Eq. (15) we have slope $S_3 = h_1^2(p+q)/(BR_1) = 0.0051 \pm 0.0008$ and intercept $I_3 = h_1^2/(BR_1)(-p \ln h_1 - q \ln R_1 + D) = -0.0157 \pm 0.0026$, both in good agreement with the direct-fitted values from plot. These tests verify the self-consistency of our data and the validity of the form of the force equation, thus supporting the scaling behavior of R_c.

The useful information we obtain from these tests concerning the scaling exponents is the relation between p and q. We cannot determine the value of λ in Eq. (13) just from these tests. However, geometrical measurements show that R_c varies very little with R_p. Indeed, we find that the standard deviation of values of R_c at different R_p is only about a couple percents of the mean value of R_c. It seems this observation serves as a good footing for us to believe that R_c is

TABLE I. Results of the testing force equation for different values of ϵ.

ϵ	Determinant	B/p	p
0.10	0.016 ± 0.861	0.547 ± 0.005	0.355 ± 0.053
0.15	-0.053 ± 0.973	0.367 ± 0.003	0.344 ± 0.040
0.20	0.056 ± 2.076	0.267 ± 0.001	0.381 ± 0.071
0.25	0.163 ± 2.720	0.203 ± 0.001	0.410 ± 0.073

independent of R_p. If we make this assumption—that is, if we take $\lambda = 0$—then from the relation between p and q, we can obtain $p = 0.355 \pm 0.053$. This is close to the corresponding value from geometrical measurements.

Besides $\epsilon = 0.10$, we perform the above tests of the force equation for other values of ϵ. The results are summarized in Table I. We notice that all the values of p are consistent with scaling exponent of $1/3$. In addition, by comparison of Eqs. (13) and (15), it is easy to see that B is inversely proportional to ϵ. This relation can be readily confirmed from the data shown in the table.

As mentioned in Sec. II, R_c scaling is expected to break for sufficiently large R/h. However, in our simulations discussed above, all the data are consistent with the assumption that there exists a scaling law of R_c which indicates that the asymptotic regime of large R/h is not yet reached. The values of R/h in our simulations vary between 100 and 500. We conclude that the lower limit of this asymptotic regime should be at least above 500. It is unsettling that the asymptotic regime should require such large R/h, but similar behavior occurs in related phenomena. For example, the asymptotic scaling of the stretching ridge requires a ratio of R/h of over a thousand [4].

The reason for this unusually high lower limit may be the following. The minor radius of the crescent is expected to be asymptotically much smaller than R_c. However, our observation shows that this minor radius is comparable with R_c for the range of R_c/h we are able to simulate. In this respect we see directly that our system is not asymptotic. We have noted in Sec. II that the system's asymptotic behavior depends strongly on how this minor radius behaves. Thus one cannot expect asymptotic scaling of R_c without asymptotic behavior of the minor radius. Since our simulations do not reach this behavior, we should not be surprised that R_c may not show asymptotic scaling, either. To demonstrate that the minor radius is not asymptotic, we show its behavior in Fig. 8. This plot shows the intersection of the surface with a vertical plane passing transverse to the crescent. Thus the radius of curvature of this curve at its peak is the minor radius. Both the horizontal and vertical scales are normalized by R_c. It is evident from the plot that this normalized width is on the order of unity for all of the four thicknesses; this means that the minor radius of the crescent is comparable with R_c. In addition, the feature that the minor radius of the crescent relative to R_c is growing smaller as the thickness decreases provides evidence that the observed scaling behavior of R_c in our simulations is nonasymptotic.

IV. DISCUSSION

In this paper we have explored the properties of the conical singularity of a developable cone, especially the scaling
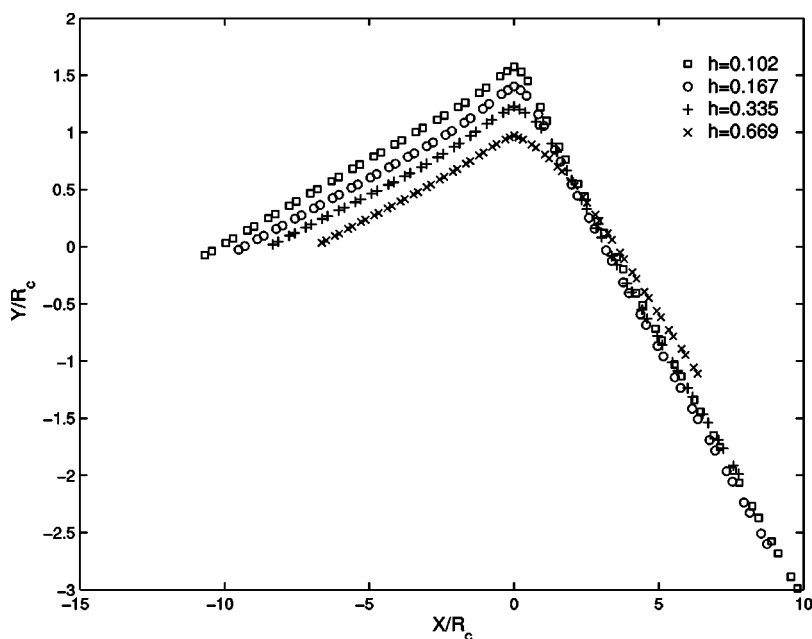
FIG. 8. Intersections of a d cone with a vertical plane consisting of its maximally deflected line and z axis, for four different thicknesses. Only the region near the peak is shown here. Both scales are normalized by the corresponding R_c for values of h as indicated in the legend. Thicknesses are in the units of lattice spacing a.

of the core region size. We have found two types of stresses in the outer region of a single d cone that scale differently with the distance to the tip. One type of stress arises from the normal force balance of the sheet without the external load and scales as $1/r^2$. The other type of stress scaling as $1/r$ is needed to balance the external pushing force. However, it is revealed that the contribution of both stresses to the stretching energy is negligible compared with bending energy of the outer region.

We also examined the normal force pressure from the container. The jump in the curvature derivative $\dot{\phi}/r$ requires a δ-function pressure from the container edge at the take-off points. We verified that this singular pressure is present with the predicted magnitude [12]. As a consequence, a substantial fraction of the container forces comes from this δ-function term.

Our numerical tests of pushing force equation suggest the existence of scaling behavior of R_c in the regime we studied—that is, when R is comparable with R_p. We obtain a simple proportionality factor between exponents p and q. Since R_c has a dependence on h—i.e., p is nonzero—it follows that q is nonzero, which implies that R_c must have a dependence on R. This is somewhat counterintuitive. Moreover, geometrical measurements of core size provide suggestive numerical evidence that R_c is independent of R_p. By

taking this assumption, we are led to a scaling law suggesting $R_c \sim h^{1/3} R^{2/3}$. Although our numerical results are consistent with the scaling prediction of Ref. [5], we were unable to justify the arguments leading to their prediction. The factors determining R_c are necessarily subtle, since the dominant energy B_0 depends only logarithmically on R_c. Until a clear justification for this scaling can be found and validated, the apparent scaling we observed must be viewed as provisional.

Our work in progress aims to explore the energetics leading to R_c scaling in more details. Our preliminary findings suggest new features that may help to resolve this issue. First, one may construct variants of a d cone that require no forcing at the core. Our preliminary data show that these variants have qualitatively different scaling behavior than the conventional d cones. Second, conventional d cones appear to obey an unanticipated constraint at the container edge. The mean curvature appears to vanish there for a wide range of d-cone shapes. We anticipate that the energy focusing in d cones will prove to be rich and revealing.

ACKNOWLEDGMENTS

[1] A. E. Lobkovsky, Phys. Rev. E **53**, 3750 (1996).
[2] A. E. Lobkovsky and T. A. Witten, Phys. Rev. E **55**, 1577 (1997).
[3] A. E. Lobkovsky, S. Gentes, H. Li, D. Morse, and T. A. Witten, Science **270**, 1482 (1995).
[4] T. A. Witten and H. Li, Europhys. Lett. **23**, 51 (1993).
[5] E. Cerda, S. Chaieb, F. Melo, and L. Mahadevan, Nature (London) **401**, 46 (1999).
[6] E. Cerda and L. Mahadevan, Phys. Rev. Lett. **80**, 2358 (1998).
[7] M. Ben Amar and Y. Pomeau, Proc. R. Soc. London, Ser. A **453**, 729 (1997).
[8] S. Chaieb, F. Melo, and J.-C. Geminard, Phys. Rev. Lett. **80**, 2354 (1998).
[9] S. Chaieb and F. Melo, Phys. Rev. E **60**, 6091 (1999).

[10] A. Boudaoud, P. Patricio, Y. Couder, and M. Ben Amar, Nature (London) **407**, 718 (2000).

[11] T. Mora and A. Boudaoud, Europhys. Lett. **59**, 41 (2002).

[12] E. Cerda and L. Mahadevan (unpublished).

[13] D. J. Struik, *Lectures on Classical Differential Geometry* (Addison-Wesley, Reading, MA, 1961).

[14] E. H. Mansfield, *The Bending and Stretching of Plates* (Pergamon, New York, 1964).

[15] H. S. Seung and D. R. Nelson, Phys. Rev. A **38**, 1005 (1988).

[16] L. D. Landau and E. M. Lifshitz, *Theory of Elasticity* (Pergamon Press, New York, 1986).

[17] W. H. Press, S. A. Teukolsky, W. T. Vetterling, and B. P. Flannery, *Numerical Recipe in C* (Cambridge University Press, Cambridge, England, 1996).

[18] B. A. DiDonna, Phys. Rev. E **66**, 016601 (2002).